Conf-9208142--6

Presented at the 14th Intl. FEL Conference
Kobe, Japan - August 23-28, 1992.

BNL--47964

DE93 001974

Analysis of the Superconducting Wiggler Magnets for the ATF Harmonic Generation FEL Experiment *

X. Zhang, I. Ben-Zvi, G. Ingold, S. Krinsky, and L. H. Yu
National Synchrotron Light Source
Brookhaven National Laboratory
Upton, NY 11973

Received OSTI

OCT 26 1992

Abstract

In this paper, we consider the superconducting wiggler magnet under construction for the High Gain Harmonic Generation experiment (HGHG) at the Accelerator Test Facility (ATF) at BNL. This wiggler consists of an energy modulation section, a dispersion magnet and a radiator section. We present an analysis of the dispersion magnet and the of end effects in the other wiggler sections. The purpose of the dispersion magnet is to convert energy modulation of the electron beam into spatial bunching. For the dispersion magnet, we discuss the physical requirements, analyze the magnetic design, determine the focussing properties, and consider the effect of departures from ideal behavior on the FEL gain. In the modulator and radiator wigglers we analyze the effects due to the ends of the wiggler and discuss their correction. In addition, the localized field produced by a trim coil for horizontal beam steering is investigated.

I Introduction

The High Gain Harmonic Generation experiment (HGHG) [1] at the Accelerator Test Facility (ATF) at BNL [2] will provide a proof of principle for the design of a proposed UV-FEL User Facility [3, 4]. In the experiment it is planned to triple the frequency of a CO_2 seed laser by utilizing two superconducting wigglers separated by a dispersion section as shown in Fig. 1. The first wiggler, resonant to 10.4 μm, is used to modulate

*This work was performed under the auspices of the U.S. Department of Energy.

the energy of the electron beam through the ponderomotive force resulting from the CO_2 seed laser. In the dispersion section, the particles with higher energy will be deflected less effectively and thus travel a shorter path length than those with lower energy. As a result, the electrons are bunched. This coherent spatially bunched beam induces superradiant emission at the third harmonic when it passes through the second wiggler, which is tuned to resonate at this harmonic. Characteristically, along the second wiggler the radiation initially grows quadratically, then exponentially in an untapered section and quadratically again in a tapered section after saturation.

The radiator is 151.2 cm long wiggler with a total of 84 periods. The period length is 18 mm and the full gap of the wiggler is 8 mm. A parabolic shape cut at the inside surface of the wiggler pole provides nearly equal focussing in both horizontal and vertical planes. The ferromagnetic yoke of the wiggler is machined out of a solid block of low carbon steel. A superconducting NbTi coil is wound continuously along the yoke, with the winding direction alternating every half period. The wiggler is under construction by a collaboration between BNL and Grumman. The advantages of this superconducting wiggler are:

a) high magnetic field;
b) easy tuning;
c) two-dimension focussing;
d) high precision of the magnetic field distribution.

In this paper, we present an analysis of several important issues in the wiggler's design: the wiggler end effects, the design of a beam-trajectory trim-coil and the design and modelling of the dispersion section. The dispersion section design considerations are discussed in section II. A detailed design of the dispersion magnet is presented in section III. In section IV, the electron beam optics in the designed magnet is modelled and its effects on the FEL are examined. In section V, we begin with the discussion of the ideal periodic wiggler with infinite periods. On the basis of this ideal case, we examine the effects due to the end of the wiggler and discus their compensation. We then turn to the study of generating a localized field distribution for particle orbit correction in section VI.

II Dispersion Section Design Consideration

The dispersion section is used to convert an energy modulation produced in the first wiggler into a spatial bunching. The ideal dispersion section is an achromat in which the longitudinal phase $[\psi \equiv (k_s + k_w)z - \omega_s t]$ of a particle changes in proportion to the deviation from the average energy,

$$\Delta\psi = \frac{d\psi}{d\gamma}\Delta\gamma. \tag{1}$$

We assume a two-dimensional magnetic field whose vertical component B is expressed in terms of the horizontal component of the vector potential A by $B = \partial A/\partial z$. The path length s in the mid-plane can be written in terms of particle momentum p and vector potential A [5]

$$s(z) = \int_{-\infty}^{z} \frac{a_0}{\sqrt{a_0^2 - A(z')^2}} dz', \tag{2}$$

where $a_0 = p/e$. Using the paraxial and highly relativistic approximations, the dispersion can be written as a function of the vertical magnetic field in the magnet [6]

$$\frac{d\psi}{d\gamma} = k_s \frac{ds}{d\gamma} = \frac{e^2 k_s}{m^2 c^2 \gamma^3} \int_0^{L_d} dz \Big[\int_0^z dz' B(z')\Big]^2. \tag{3}$$

where k_s is the resonant wavenumber of the second wiggler, γ is the electron beam energy, and L_d is the length of the dispersion section. The desired value of the dispersion is set by an optimization of the output radiation power. Additional conditions on the dispersion section are that the first and second integrals of the magnetic field over the distance L_d should vanish so that the beam will have no position and angular displacement resulting from the dispersion section. One example of an idealized dispersion section has a magnetic field given by

$$B(z) = \begin{cases} B_0, & 0 \le z < \frac{L_d}{4} \\ -B_0, & \frac{L_d}{4} < z < \frac{3L_d}{4} \\ B_0, & \frac{3L_d}{4} < z < L_d. \end{cases} \tag{4}$$

This field can be obtained by a system consisting of 4 identical rectangular magnets of length $L_d/4$. Obviously, this configuration satisfies the two integral conditions. The required dispersion can be achieved by adjusting the parameters B_0 and L_d. Substituting the field of Eq. (4) in Eq. (3), the dispersion is found to be

$$\frac{d\psi}{d\gamma} = \frac{e^2 k_s}{m^2 c^2 \gamma^3} \frac{B_0^2 L_d^3}{48}, \tag{5}$$

The maximum horizontal deflection x_{max} in the dispersion section is another important design parameter. Due to the symmetry of $B(z)$, x_{max} is reached at the center ($z=L_d/2$) of the dispersion section. This maximum value in the mid-plane is given by

$$x_{max} = 2\rho(1 - \cos\theta), \tag{6}$$

where ρ is the bending radius in the magnet and

$$\sin\theta = \frac{L_d}{4\rho}.$$

For $L_d/4\rho \ll 1$, $1 - \cos\theta \approx \theta^2/2$ and $\theta \sim \sin\theta \approx L_d/4\rho$, then

$$x_{max} \approx \rho\theta^2 \approx \frac{B_0 L_d^2}{16mc\gamma}. \tag{7}$$

Table 1: System Parameters in the ATF HGHG Experiment [(1) and (2) stand for first wiggler and second wiggler respectively].

Energy, [MeV]	30
Peak Current, [Amp]	110
Normalized RMS Emittance,[mm-mrad]	4.0
RMS Energy Spread [%]	0.0435
e-beam Edge Radius (1)[mm]	0.424
e-beam Edge Radius (2)[mm]	0.525
Resonant Wavelength (1)[μm]	10.42
Betatron Wavelength (1)[m]	1.608
Wiggler period (1)[mm]	26
Resonant Wavelength (2)[μm]	3.47
Betatron Wavelength (2)[m]	2.466
Wiggler period (2)[mm]	18
Wiggler gap (1,2)[mm]	8

Under this assumption of a small bending angle, it is seen that the maximum deflection is inversely proportional to the energy of the particles.

The related system parameters in the HGHG experiment, currently under construction, are listed Table 1. To minimize the wakefield effects, we choose the gap of the dispersion section to be the same as that of the other two wigglers. The horizontal pole width should be enough to keep constant field up to the maximum deflection. From Eqs. (5) and (6), for a fixed dispersion $d\psi/d\gamma$ and a given electron energy γ, the choice of higher magnetic field with shorter length of dispersion section minimizes x_{max}. The length of the dispersion section in the HGHG experiment is 10 cm.

III Magnetic Design and Results

We have studied the dispersion, steering and displacement in the dispersion magnet design using the 2-D computer code POISSON. Our dispersion section is a single period electromagnetic wiggler with a uniform gap. The the right-upper quarter of the dispersion magnet is shown in Fig. 2. The rest is determined by the symmetry of the system. The boundary conditions are Dirichlet on the left boundary and Neumann on the right, upper and lower boundaries.

Following a suggestion of K. Halbach [5], we use field clamps at the ends of the dispersion section to reduce the fringe fields leaking out from the magnet ends. Thus there are five iron poles, one long main pole, two side poles and two end poles that serve as field clamps. Three coils with equal currents are wound around the three magnetic field poles. The ratio of the width of the side pole to main pole is slightly different from 1 . 2 : 1 to make the first field integral vanish over the half dispersion section. The second integral vanishes automatically by symmetry.

The field clamp provides a low reluctance connection between the upper and lower end poles, placing them at scalar potential equal to that of the mid-plane. Window-frame type field clamps are connected at the both ends of the magnets. To simulate the 3-dimensional field clamp using the 2-dimensional program POISSON, we use a procedure developed by Halbach [5]. A fictitious iron bar with infinite permeability connects the outer edge of the dispersion magnet to the right boundary, as shown in Fig. 3. This makes integral $\int \vec{H} \cdot \vec{dl}$ from the magnet end to the mid-plane vanish, since the right end of the problem has a Neumann boundary condition. This places the end pole at equal scalar potential to the mid-plane. In the regime of low saturation, the field in the body of the magnet is only slightly modified by the field clamp since little flux passes through the clamp.

The field line plot of the dispersion magnet is shown in Fig. 3. In this calculation, we use the variable permeability table for the magnet iron and large ($\mu = 1 \times 10^5$), constant permeability for the field clamp bar. The coils are excited with 2800 : 5600 Ampere-turns to provide $d\psi/d\gamma = 22$ as required by the experiment. Note that there are no field lines inside the simulated field clamp. The field in the mid-plane of the half magnet is shown in Fig. 4. The field amplitude at the central pole is approximately equal to that at the side pole, but the polarity of the field is inverted. The field vanishes quickly in the field clamp pole.

The field in the mid-plane and the dispersion are displayed as a function of the coil excitation in Fig. 5. With an excitation of 5000 Ampere-turns, the magnet generates 1.4 Tesla peak field and a dispersion $d\psi/d\gamma$ of 50, while operating almost in the linear region. The first field integral in the half magnet which is nearly zero at the nominal current, is about 60 Gauss-cm at an excitation of 5000 Ampere-turns. This corresponds to 0.6 mrad beam steering. Since this value is about twice the tolerance required by the experiment, a pair of small trim coils would be needed if the dispersion has to be adjusted to such an extreme value.

The coils are made of superconducting wire with a diameter of 0.44 mm. The main coils are twice the size of the side coils, which have area $5 \times 3\ mm^2$. The number of turns in the side coil is 63. The excited current per turn is below 80 Ampere, well below the short sample quench current, which is over 200 Amperes.

This dispersion magnet can also be used in the proposed NSLS UV-FEL, where the typical radiation wavelength is 100 nm and electron beam energy is 260 MeV. With 6 mm gap and 2800 : 5600 Ampere-turns coil excitation, the magnet can generate field with peak value 1.156 T and produce the dispersion of 2.5 needed for that device.

IV Beam Optics in the Dispersion Section

The dispersion section is designed with no horizontal focussing. As a result, the beam can only be matched to one of the two wigglers. This effect may cause some reduction of the FEL radiative power. To estimate this effect, we have to determine the transport matrix of the dispersion section.

For this purpose, the dispersion wiggler is modelled by a collection of dipole magnets and drifts. Since the first and second field integrals are equal to zero, we use three rectangular dipoles (B1, B2 and B3) to form an achromatic bending device. The value of the dipole field is taken from the POISSON calculation. The length of the dipole magnet is adjusted to make the field integral over each rectangular pole equal to the integral found by POISSON for the true geometry. The drifts (D1 between the end plane and B1 or B3, and D2 between B2 and B1 or B3) make up the extra space. The parameters of these elements are listed in Table 2. Since the field between the poles does not follow a step function-like jump, the hard edge model of the dipole magnet overestimates the focussing effects in the vertical plane due to the fringe field. Therefore, we employ a correction term K_1 to take into account the spatial extent of fringing fields [8].

$$K_1 = \int_{-\infty}^{\infty} \frac{B(z)(B_0 - B(z))}{g B_0^2} dz, \tag{8}$$

where $B(z)$ is the magnitude of the fringing field on the mid-plane at a position z, B_0 is the asymptotic value of $B(z)$ inside the magnet, and g is full gap of the bending magnet. The values of K_1 are given in Table 2.

Table 2: Parameters of the modelled dispersion section.

Component	Length (cm)	Field (T)	K_1 (in)	K_1 (out)
D1	4.93			
D2	0.45			
B1	1.81	0.876	0.35	0.25
B2	3.62	0.876	0.25	0.25
B3	1.81	0.876	0.25	0.35

The transport matrix shown in Eq. (9) was produced by the TRANSPORT code, which includes the drift spaces between the dispersion section and the two wigglers

$$R = \begin{pmatrix} 1.00002 & 0.18074 & 0.00000 & 0.00000 & 0.00000 & 0.00000 \\ 0.00025 & 1.00002 & 0.00000 & 0.00000 & 0.00000 & 0.00000 \\ 0.00000 & 0.00000 & 0.67546 & 0.15184 & 0.00000 & 0.00000 \\ 0.00000 & 0.00000 & -3.58112 & 0.67546 & 0.00000 & 0.00000 \\ 0.00000 & 0.00000 & 0.00000 & 0.00000 & 1.00000 & 0.00739 \\ 0.00000 & 0.00000 & 0.00000 & 0.00000 & 0.00000 & 1.00000 \end{pmatrix}. \tag{9}$$

This matrix shows that the dispersion section behaves nearly as a drift horizontally and as a thick focussing lens vertically. Converting the R_{56} term (in units $mm/\%$)

in the matrix to dispersion, the result is in good agreement with the value calculated from Eq. (3) using the detailed field distribution from the POISSON output. In addition, the maximum deflection occurring at the symmetric plane of the dispersion wiggler is 3.4 mm, also in agreement with the POISSON result. Using this model we can investigate second order effects on the longitudinal phase shift, such as the effects due to transverse position and angle of the beam. The results given by TRANSPORT show that second order effects are negligibly small.

In the HGHG experiment, the beam is matched to the radiator wiggler, but not to the first wiggler. Using the transport matrix of the dispersion section and the first wiggler, we can work out the required beam phase space parameters at the entrance of the first wiggler. To determine the effect on the radiated output power, a simulation using code TDA [9] was employed with the calculated transport matrix and beam parameters. The result showed there was no significant reduction of the FEL radiated power due to the lack of matching into the first wiggler.

V Wiggler End Effects

In the following sections we deal with the design of the wiggler magnets. It is worthwhile to have a brief discussion of the performance of a wiggler with an infinite number of periods before dealing with end effects and trim coils. In the case of periodic boundary condition and finite permeability, a sine-like field is generated with the period equal to the wiggler wavelength. In the mid-plane, the peak field is 0.578 T for a current of 6 kA-turns.

The peak field vs the excited current is plotted in Fig. 6. Clearly, the wiggler starts saturating when the current exceeds 3 kA-turns. The HGHG experiment is designed to operate at a peak field of 5.8 k-Gauss, corresponding to a current of about 6 kA-turns. In this case saturation reduces the field by about 24%.

To reduce the angular and displacement errors, we use a binomial excitation pattern [7] of order 3, i.e., the coils are excited with a pattern of $1 : -3 : 4 : -4 : 4 : -4 : \cdots$, starting from the end of the wiggler. This compensation scheme requires the wiggler to have an odd number of poles and an even number of coils. The fictitious iron bar [5] with a large constant permeability ($\mu = 1 \times 10^5$) connecting the end pole to the left boundary is simulating a magnetic field clamp.

Due to the end effect, the field is seen to reach its equilibrium value after 1 to 2 wiggler periods. Due to saturation, the first field integral is about 650 Gauss-cm for a current of 6 kA-turns, (equivalent to giving 6.5 mrad angular kick) in spite of the binomial excitation pattern.

To compensate the angular kick, a pair of extra correction coils are added on each side of the first field pole. When the current in these coils are adjusted to 240 A-turns (the current initially is 1500 A-turns in the first coil), the first field integral essentially vanishes. The field lines and the field in the mid-plane including the correction are plotted in Figs. 7 and 8, respectively. With the correction, there are no field lines passing through the field clamp, although a few field lines pass through it in the case of no correction. As we expected, the correction coils mainly affect the fields in the region of first and second poles making the first field integral vanish. In addition, a nonzero second field integral is seen. Clearly, the electron trajectory will have a constant displacement associated with this second integral when it goes through the wiggler end. In the case with compensation, the second integral is about 1000 $Gauss - cm^2$ and it can introduce about 0.1 mm centroid shift for our 30 MeV beam.

To reduce the displacement associated with the second integral, the 4th binomial excitation may be used, with a pattern of $1 : -4 : 7 : -8 : 8 : -8 : \cdots$. To have this pattern, the wiggler must contain an even number of poles and an odd number of coils. The pole scalar potentials are $1 : -3 : 4 : -4 : 4 : \cdots$. The field along the z-axis is anti-symmetric and the potential is symmetric about the center coil, which is different from the case of order 3, where the field is symmetric and the potential is anti-symmetric about the center pole. Using a POISSON simulation in the regime of low saturation, we have verified that this pattern is steering-free and displacement-free as expected.

VI Design of Trim Coil

Errors in the wiggler magnetic field may cause an electron beam centroid shift (transversely) and an electron phase deviation (longitudinally). In either case, the errors may reduce FEL gain and radiated power. Since errors in the real wiggler are inevitable, their correction is necessary. Furthermore, in the case of the HGHG experiment, the latter part of the second wiggler is tapered for maximum energy extraction from electron beam. The steering error in the transition between wiggler sections with unequal currents is minimized using the 3rd order binomial coefficient in each transition. This angular error can reach 0.3 mrad for 30 MeV beam. The correctors along the wiggler are conservatively designed to provide about 3 mrad angular kick.

A magnetic correction produced by a trim coil is suitable for the correction in a superconducting wiggler. The trim coil is superimposed on the main coil in the wiggler. For a 3-mrad angular kick, the trim coil should generate a localized magnetic field with a field integral of 300 Gauss-cm. To eliminate the change in the trajectory length due to the trim coil, the trim coil should cover an even number of poles [5], The change in trajectory length $\Delta S(z)$ can be divided into three parts [5],

$$\Delta s(z) = x_0(z)\Delta x'(z) - \int x_0(z)\Delta x''(z)dz + \frac{1}{2}\int \Delta x'^2(z)dz.$$

Here, x_0 is particle horizontal position given by the original wiggler magnetic field. $\Delta x'$ and $\Delta x''$ are the angular kick and its derivative respectively, which are introduced by the field increment ΔB produced by trim coil. The first term vanishes if evaluated at the positions of integer number of the periods. If the field increment ΔB is a symmetric with z-coordinate and x_0 is a anti-symmetric, and if the integral is carried out over an integer number of wiggler periods, then the second term vanishes. The last term always exists since the integrand is definite positive. However, this term may provide a cancellation of similar term introduced by the wiggler errors, which the trim coil is designed to correct.

The trim coil is powered by 100 Ampere-turns and covers 2 poles. The field produced by the trim coil and has very local effects, mainly at poles covered by the trim coil. With 100 Ampere-turns the first field integral in the trim coils is close to 300 Gauss-cm. In the region of small excitation, we find that the field integral is nearly linear in either the excitation or the number of poles covered by the trim coil. To ensure the proper positioning of the electron beam centroid in the ATF HGHG experiment, 6 trim coils will be set along the superconducting wiggler with equal spacing. Each of them will cover 4 poles to reduce the driving power for the trim coil current.

ACKNOWLEDGMENTS

We express our thanks to K. Halbach for many suggestions and consultations, and to D. Li for the FEL numerical simulations.

symmetric with z-coordinate and x_0 is a anti-symmetric, and if the integral is carried out over an integer number of wiggler periods, then the second term vanishes. The last term always exists since the integrand is definite positive. However, this term may provide a cancellation of similar term introduced by the wiggler errors, which the trim coil is designed to correct.

The trim coil is powered by 100 Ampere-turns and covers 2 poles. The field produced by the trim coil and has very local effects, mainly at poles covered by the trim coil. With 100 Ampere-turns the first field integral in the trim coils is close to 300 Gauss-cm. In the region of small excitation, we find that the field integral is nearly linear in either the excitation or the number of poles covered by the trim coil. To ensure the proper positioning of the electron beam centroid in the ATF HGHG experiment, 6 trim coils will be set along the superconducting wiggler with equal spacing. Each of them will cover 4 poles to reduce the driving power for the trim coil current.

ACKNOWLEDGMENTS

We express our thanks to K. Halbach for many suggestions and consultations, and to D. Li for the FEL numerical simulations.

References

[1] I. Ben-Zvi, et al., Proc. of 1991 Intc. FEL Conf., Santa Fe, NM.

[2] I. Ben-Zvi, et al., Proc. of 1991 Intc. FEL Conf., Santa Fe, NM.

[3] I. Ben-Zvi, et al., Nucl. Inst. & Meth. **A318**, 201(1992).

[4] L. H. Yu, Physical Review A **44**, 5178(1991).

[5] K. Halbach, Personal communication.

[6] R. Bonifacio, et al., Nucl. Inst. & Meth. **A296**, 787(1990).

[7] K. Halbach, Nucl. Inst. & Meth. **A250** 95(1986).

[8] K. Brown, SLAC Report **SLAC-75** 74(1982).

[9] T. M. Tran, Comput. Phys. Commun. **54**, 263(1989).

Figure 1: Schematic diagram of the ATF HGHG experiment.

Figure 2: Detailed description of right-upper quarter of the dispersion magnet with virtual field clamp, showing dimension in mm and permeability.

Figure 3: POISSON field line plots of the dispersion magnet.

Figure 4: Field in the mid-plane vs distance, along the dispersion magnet.

Figure 5: Field in the mid-plane and dispersion vs current in the dispersion magnet.

Figure 6: The peak magnetic field vs current of the radiator wiggler.

Figure 7: POISSON field line plots of the compensated end of the radiator wiggler.

Figure 8: Field in the mid-plane vs longitudinal distance of the end-compensated radiator wiggler.

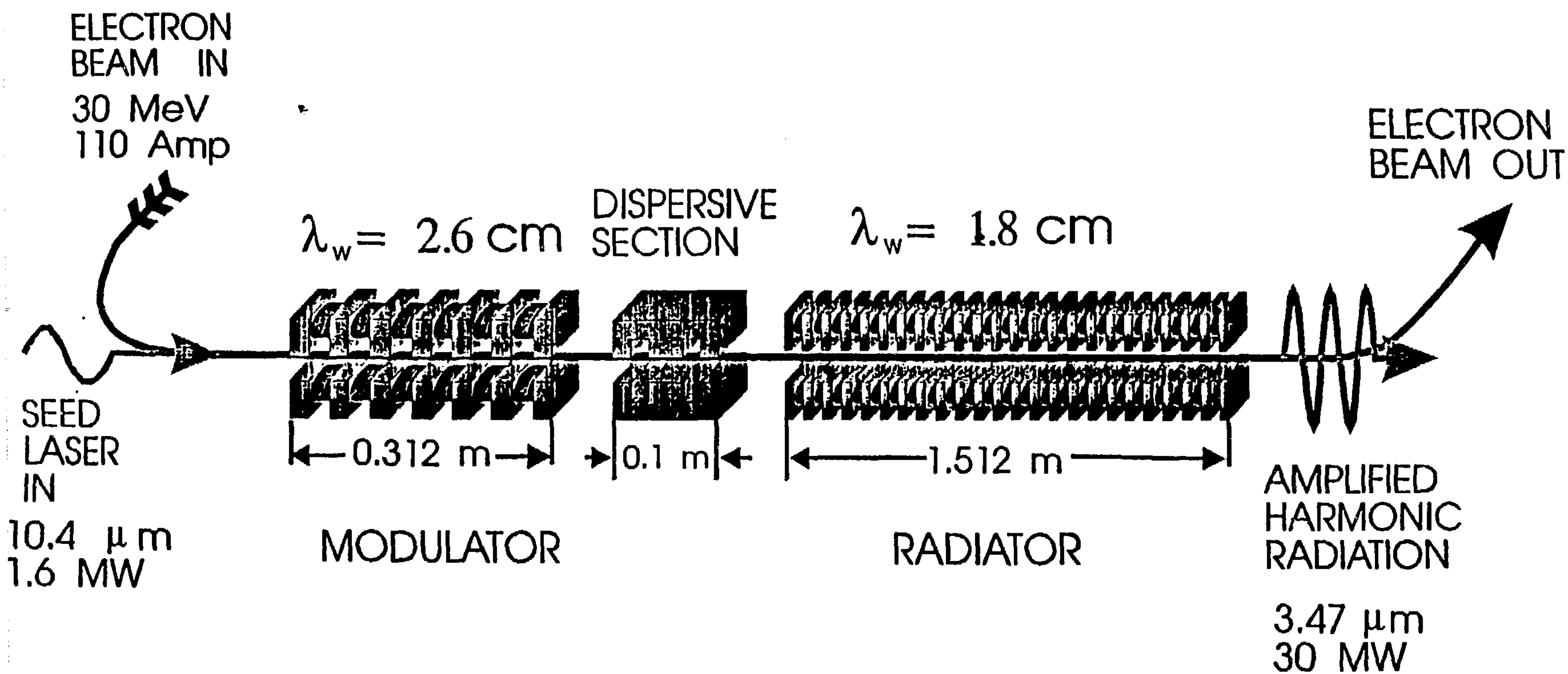

ELECTRON
BEAM IN
30 MeV
110 Amp
SEED
LASER
IN
10.4 µm
1.6 MW
λw= 2.6 cm
DISPERSIVE
SECTION
λw= 1.8 cm
0.312 m
0.1 m
1.512 m
MODULATOR
RADIATOR
ELECTRON
BEAM OUT
AMPLIFIED
HARMONIC
RADIATION
3.47 µm
30 MW

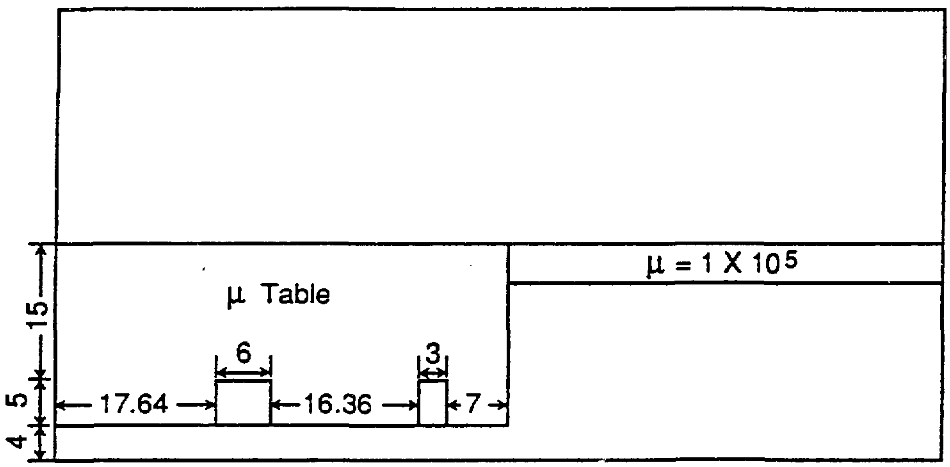

Zhang 2 7/92 IR

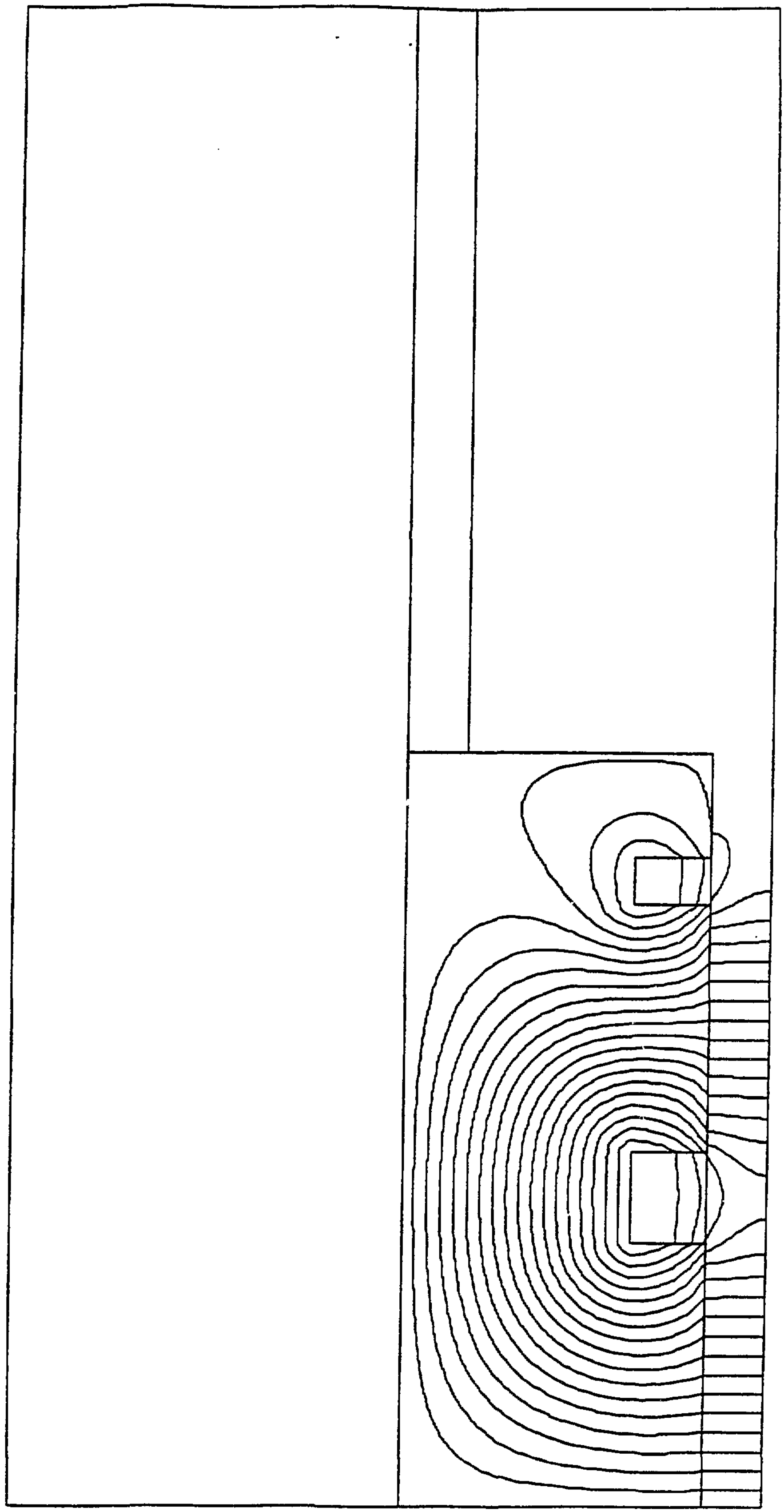

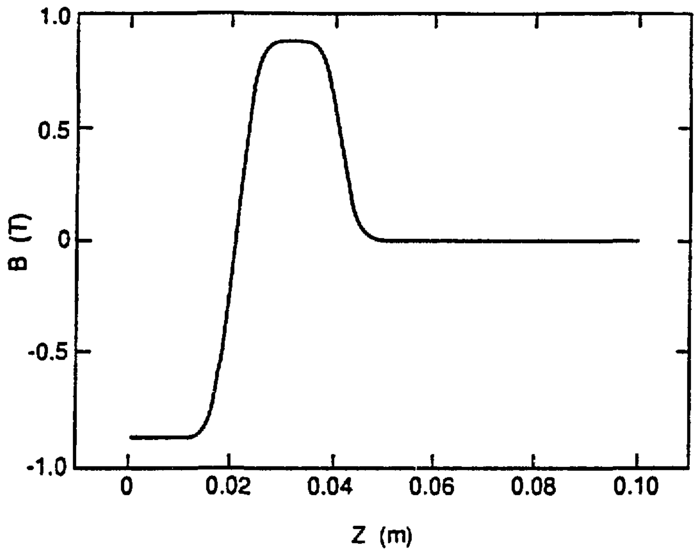

Zhang 5a 7/92 IR

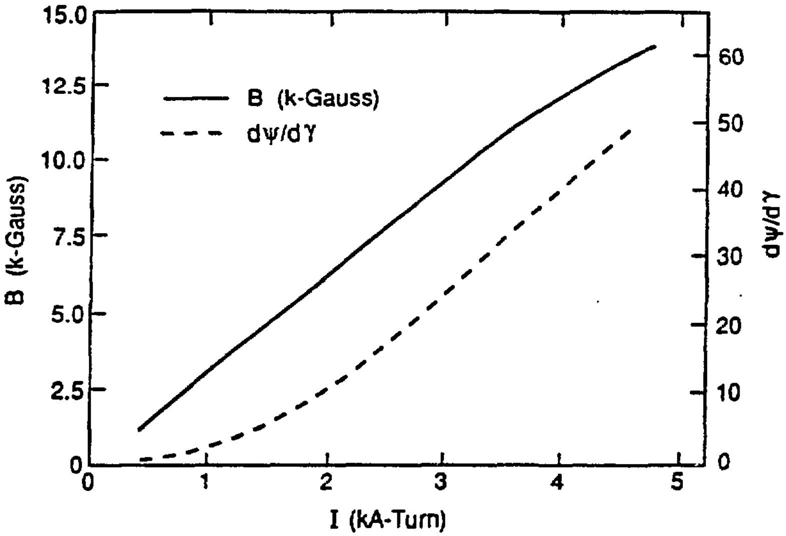

Zhang 6a & 7a 7/92 IR

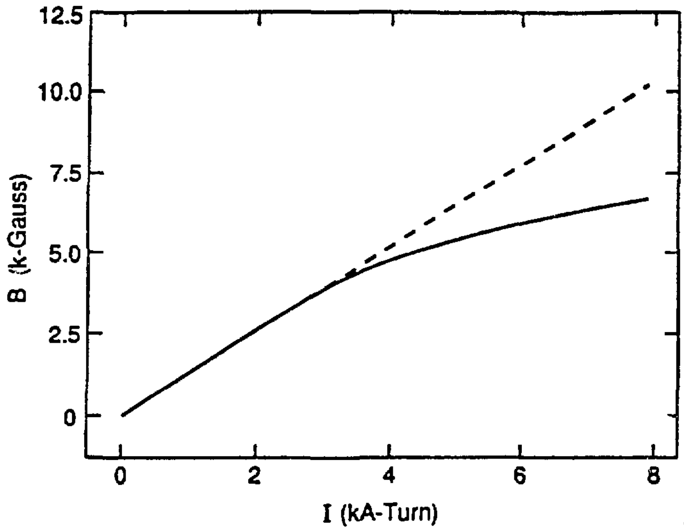
12.5
10.0
7.5
5.0
2.5
0
B (k-Gauss)
0
2
4
6
8
I (kA-Turn)

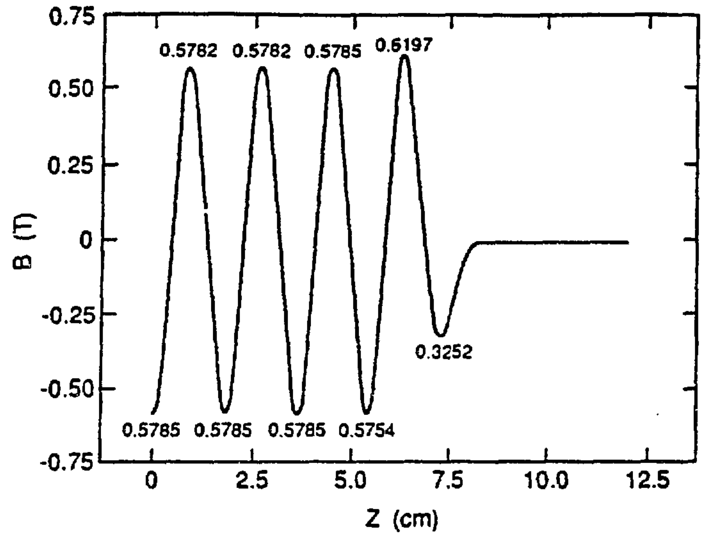

Zhang 8 7/92 IR